Effects of External Flow near High-Current Hollow Cathodes on Ion-Energy Distributions

Ikuya Kameyama* and Paul J. Wilbur†
Colorado State University
Fort Collins, CO 80523

Abstract

The effects of ambient pressure and external flow introduced immediately downstream of hollow cathodes on ion currents with energies greater than that associated with the cathode-to-anode potential difference were investigated using an electrostatic energy analyzer. Either increasing the ambient pressure or adding external flow induces an increase in the distribution of ion currents with moderate energies ($< \sim 30$ to ~ 35 eV) and a decrease in the distribution for high energies ($> \sim 30$ to ~ 35 eV). A scattering model of high-energy ions in ambient plasma was developed to estimate the effects of neutral density for an MHD model. The results showed, however, that this model involves no mechanism by which a significant increase in ion current could occur at any energy. It was found, on the other hand, that the potential-hill model of energetic-ion production, which assumes the existence of a local maximum in plasma potential, could explain observed increases and decreases in moderate and high energy currents, respectively, through a charge-exchange mechanism.

Introduction

Steady improvement in space electric power generation technology have made high-power, high-thrust ion-propulsion systems, which require high-current hollow cathodes, more viable. It was found, however, that severe sputter erosion on various electrodes and structures located near hollow cathodes operating at high emission currents (a few tens of amperes) could limit the lifetime of an ion-propulsion system.[1,2] Some experiments were conducted to measure energy distributions of ions from high-current hollow cathodes to identify causes of this erosion and they revealed ions with high energies emanated from high-current hollow cathodes.[3,4,5]

An experiment was conducted to measure erosion rate distributions on copper as a function of zenith angle (the angle measured from the cathode centerline toward a direction parallel to the orifice plate plane).[6] In these experiments, it was shown that erosion rates were reduced dramatically over the entire range of zenith angles investigated by introducing additional expellant flow into the region immediately downstream of the cathode orifice. This result was applied to the NSTAR (NASA Solar Electric Propulsion Technology Application Readiness) thruster design, which after 867 hours of a 2000-hour test showed severe erosion on the cathode orifice plate and the cathode heater which protruded downstream of the orifice plate plane.[7] An enclosed keeper was installed, thereby increasing the neutral density around the cathode and inducing the beneficial effect of additional flow as described in Ref. 6. Preliminary results suggest this change has mitigated the NSTAR thruster erosion problem.[8]

In this paper, ion-energy distributions were probed using an ESA as ambient neutral density and external flow rate were changed. Effects of changes in neutral density downstream of high-current xenon hollow cathodes on the energy distributions of ions emitted from the cathodes are presented.

Experimental Apparatus and Procedures

The physical arrangement of components used in this study and shown in Fig. 1 is identical to that for previous studies[5,6] except the size of the cathode orifice. The 6.4-mm-diameter, orificed hollow cathode had an orifice with minimum and maximum diameters of 0.81 and 1.47 mm near its upstream and downstream ends, respectively. The cathode was surrounded by the 60-mm-inner-diameter-by-115-mm-long, water-cooled, copper anode as shown in Fig. 1. The anode extended beyond the top end of cathode about 75 mm and had an ~ 35-mm-wide slit on one side through which the cathode discharge could be observed.

* Research Assistant, Dept. of Mech. Engr., Student Member AIAA and JSASS
† Professor, Dept. of Mech. Engr., Member AIAA

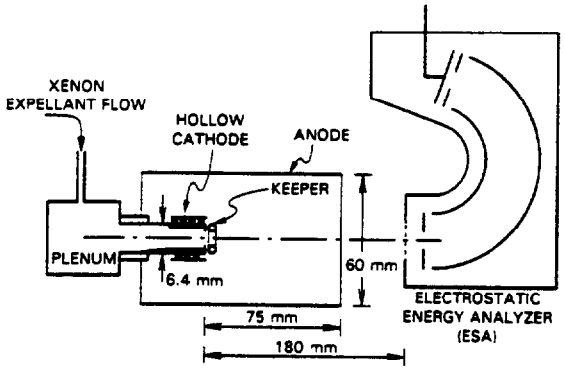

Fig. 1 Experimental Setup

The cathode insert (a low-work-function electron emitter) was made of a rolled tantalum foil with a tantalum ribbon attached to enable electrical contact and hold the insert in place. The rolled foil was dipped in a solution containing barium carbonates (Chemical R-500) and inserted into the cathode tube. Sintered tungsten inserts, which are generally used in flight-qualified hollow cathodes, were not investigated because previous research had shown insert type did not affect ion-energy distributions significantly.[9] A swaged tantalum heater was friction fitted to the cathode tube and tantalum foil heat shields were also used to reduce the radiation heat loss from it. The keeper electrode was constructed from a 1.5-mm-diameter tantalum wire that was bent into a 4.0-mm-inner-diameter toroidal ring and positioned 1.0 mm downstream of the cathode orifice. In order to prevent transient discharges between the cathode plasma and facility ground, the hollow-cathode/anode assembly was floated. The cathode-to-ground potential difference was typically almost constant at 0 ~ 5 V during each test.

The electrostatic energy analyzer (ESA) used to measure energy distributions of ions produced in hollow-cathode discharges for these tests and those described in Refs. 5 and 10 was positioned 180 mm downstream of the cathode orifice with its entrance-collimator axis aligned with the cathode axis (i.e. looking at the cathode orifice). The unit had a 2.0-mm-diameter, active current-collection area at its entrance collimator. In order to sense an ion-current energy distribution, internal conditions were set to detect 10-eV kinetic energy ions in the ESA and the potential of the entire unit was swept with respect to facility ground potential. Uncertainties in these measurements are discussed in Ref. 11.

In order to examine effects of the neutral density environment downstream of the cathode on the ion-energy distributions, the ambient pressure, P_0, was raised by throttling the flow through a gate valve located between the vacuum chamber and the cryopump in some tests. In other tests, externally supplied xenon was injected toward the orifice through tubes arranged as shown in Fig. 2 while ambient pressure was held constant.

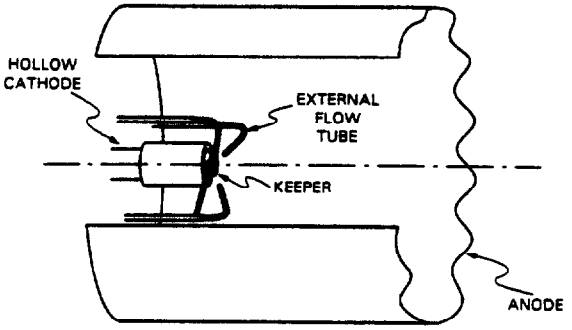

Fig. 2 Setup for External-Expellant-Flow Experiment

Xenon was supplied through the tubes rather than as increased orifice flow so the xenon atom density near but outside of the orifice would be changed but plasma properties and neutral densities inside the cathode and cathode orifice would not. The ends of the three, nickel tubes (0.51 mm i.d. by 0.81 mm o.d.) were ~5 mm downstream of the orifice. The tubes were isolated from adjacent equipment using ceramic tubes so they would float electrically and their influence on plasma properties in the region would be minimized.

Neutral density profiles were measured along the cathode centerline at various ambient pressure and external flow conditions using a Shultz-Phelps ionization gauge with its glass casing partially removed to expose its active elements. The gauge was calibrated in a room-temperature, xenon atmosphere using a McLeod (high-vacuum, mercury) manometer and an assumed temperature of 300 K in the ideal gas law. Measurements were made under no-electrical-discharge conditions so that the discharge plasma would not affect the readings.

All the experiments were initiated by evacuating the vacuum chamber below 1.5×10^{-6} Torr (2.0×10^{-4} Pa) using the cryopump while the minimum ambient pressure achieved at zero xenon flow was of the order of 10^{-7} Torr (10^{-5} Pa). When the neutral density profiles were obtained, the xenon flow rates through orifice and capillary tubes ($\dot{m}_c$ and $\dot{m}_{ext}$, respectively) were set and the gate valve was adjusted to establish the desired ambient pressure, which was near 10^{-4} Torr (10^{-2} Pa).

The flow was stabilized for 30 minutes before any data were recorded.

Before ion-energy distributions were measured, the cathode was heated up slowly and a small amount of xenon was bled through the cathode to flush out possible contaminants. The cathode discharge was initiated by applying a high voltage to the keeper and slowly increasing the xenon flow rate through the orifice. After the keeper discharge had stabilized at 0.5 A (J_K) and ~20 V (V_K), anode power was applied. A detailed description of start-up procedures is given in Ref. 11. Once the discharge was established, operating parameters such as the cathode and external flow rates, keeper current, and discharge current (J_{CD}) were set. Discharge conditions such as discharge voltage, V_{CD}, were allowed to stabilize for at least 30 minutes before ion-current data sensed by the ESA were collected.

Density Effects in an MHD Model

One of the models which have been proposed to explain the production of high-energy ions is an MHD model first postulated by Latham, et al.[4] The MHD model would involve an abrupt plasma potential increase immediately downstream of the cathode orifice to an ambient plasma value that should be near anode potential. Hence, once the ions have passed through the orifice, in which density-change effects should be insignificant, they experience only deceleration in an adverse electric field and collisions in the ambient plasma.

The model used to predict the effects of neutral density on the scattering of high-energy ions is illustrated in Fig. 3. In the model, ions with an energy ε measured with respect to cathode potential are assumed to be created at a source located near a cathode orifice. They expand spherically into a

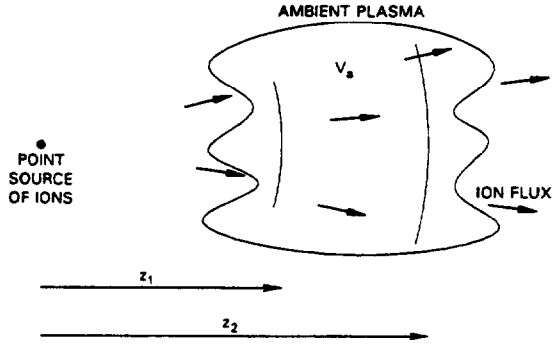

Fig. 3 Scattering Model of Ion Flux Loss due to Collisions downstream of Hollow Cathodes

downstream ambient plasma that is at a uniform plasma potential, V_a, as suggested in the figure. Some of these ions undergo collisions with neutral atoms and are scattered off of initial trajectories that would otherwise carry them to a downstream detector. The ion current associated with one kinetic energy in the ambient plasma decreases from that at a location z to that at another location $z+\Delta z$ by the factor $exp[-\sigma n_0 \Delta z]$ where σ and n_0 are total collision cross-section and neutral density, respectively. In the kinetic energy range of interest for hollow cathode applications (i.e. tens of eV) only elastic and charge-exchange collisions with neutrals are significant and it is, therefore, assumed that only these events induce significant scattering losses. In this scattering environment, the ion-current energy distributions $dJ_i(\varepsilon)/d\varepsilon$ measured using instruments with the same current-collection area and along the same path but at two different distances from the cathode, z_1 and z_2, can be related using the equation

$$\left.\frac{dJ_i}{d\varepsilon}\right|_{z=z_2} = \left.\frac{dJ_i}{d\varepsilon}\right|_{z=z_1} \frac{z_1^2}{z_2^2}\, exp\left[-\sigma \int_{z_1}^{z_2} n_0\, dz\right]. \quad (1)$$

The second and third terms in the right hand side of the equation are associated with spherical expansion and collisions, respectively.

In this work, Eq. (1) is applied twice to relate ion-current energy distributions at the same location under different neutral density profile conditions assuming that high-energy-ion production rates are independent of the downstream neutral density environment. The resulting ion-current energy distributions $dJ_i'(\varepsilon)/d\varepsilon$ and $dJ_i''(\varepsilon)/d\varepsilon$ both measured at a downstream location z_2 for neutral density profiles n_0' and n_0'', respectively, can be related to the ion-current energy distribution at a location z_1, which is very close to the cathode orifice. When no change is expected in ion production mechanisms, that is, in the ion-current energy distribution at the location z_1, these terms along with the geometrical terms cancel out and the ratio of the equations becomes

$$\frac{\left.\frac{dJ_i''}{d\varepsilon}\right|_{z=z_2}}{\left.\frac{dJ_i'}{d\varepsilon}\right|_{z=z_2}} = exp\left[-\sigma \int_{z_1 \to 0}^{z_2} \left(n_0'' - n_0'\right) dz\right]. \quad (2)$$

It should be emphasized that the left-hand side of Eq. (2) is determined from direct ion-current-

energy-distribution measurements and the right-hand side will be computed using either measured or calculated neutral density profiles.

Experimental Results

Neutral Density Profiles

In order to examine the effects of various ambient pressures and external flow rates and to incorporate the predictions derived from the models, the neutral density profiles, n_0, were measured at three different ambient pressures. The highest of these was maintained as the external flow was varied from zero in two steps by throttling the flow to the cryopump. The measurements were repeated several times to obtain mean, axial density profiles.

Figure 4 shows the effects of ambient pressure and external flow rate on the mean neutral density profiles measured. These data show that increasing the ambient pressure with no external flow yields a uniform increase in the density profile (Fig. 4a). On the other hand, introducing external flow while holding ambient pressure fixed causes a less obvious increase in the density (Fig. 4b). It was found that

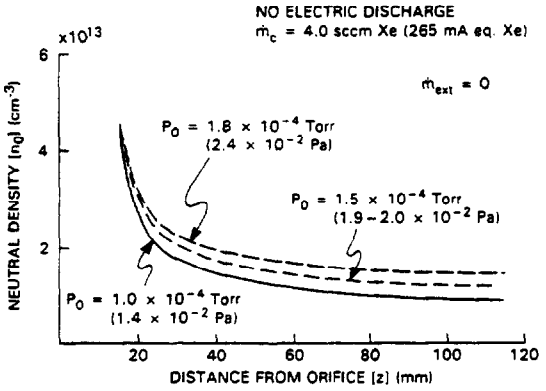

a. Effect of Ambient Pressure

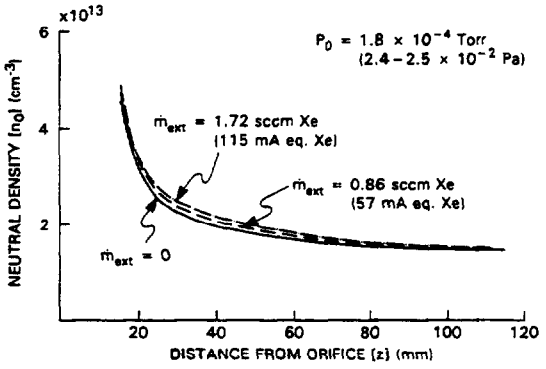

b. Effect of External Flow Rate

Fig. 4 Neutral Density Profiles Measured on the Cathode Centerline

the error ranges computed as magnitudes of standard deviations would be of the order of the line thicknesses if they were drawn in the figures. Further details of errors are discussed in Ref. 11. When the keeper was replaced with a small needle-like starter electrode, the mean density profiles were found to be similar to those measured with a keeper.

When neutral density profiles beyond this range of measurements were needed, the experimental data were extrapolated by fitting the measured profiles using three independent terms: 1) orifice flow, 2) ambient pressure, and 3) external flow. On the basis of experimental results, these density terms were represented, respectively, by 1) spherical expansion from an origin offset from the orifice, 2) linear variation with ambient pressure, and 3) exponential decay with distance from a point 5 mm downstream of the orifice. It is noted that gauge used for the measurements had large active component sizes (~1 cm along a normal to the cathode centerline) and this is expected to result in poor spatial resolution near the ~1-mm-diameter cathode orifice.

Ion-Current Energy Distributions

Typical Data and Analysis Scheme

Typical ion-current energy distribution data, which indicate the effect of changes in ambient pressure, are shown in Fig. 5a. These data, which are ion currents sensed directly by the ESA divided by its energy resolution,[10] were analyzed using Eq. (2) to obtain data suitable for comparison with scattering model predictions as shown in Fig. 5b. The analysis was accomplished by first selecting a reference distribution, $[dJ_i(\varepsilon)/d\varepsilon]_{ref}$, from among the measured ones. For the data of Fig. 5a, the one at the lowest ambient pressure (solid line) was picked. Then, normalized ion-current energy values were computed as the ratios of corresponding distribution values at each ion energy, $[dJ_i(\varepsilon)/d\varepsilon]/[dJ_i(\varepsilon)/d\varepsilon]_{ref}$. The resulting curves plotted in Fig. 5b indicate the effect of the pressure change on the ion-current distribution. For example, the normalized distribution at 1.6 x 10^{-4} Torr (dashed line) is greater than unity for energies less than ~40 eV and less than unity for energies greater than ~40 eV. This means that increasing the pressure above the reference state has induced an increase and a decrease in the ion currents at energies below and above ~40 eV, respectively. Of course, the normalized plot associated with the reference distribution in Fig. 5b is a horizontal line with a magnitude of unity.

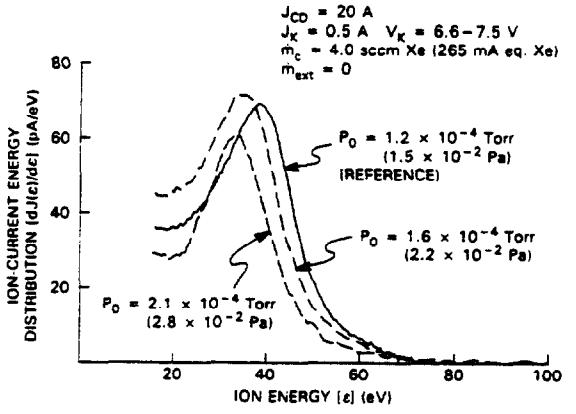

a. Measured Ion-Current Energy Distributions

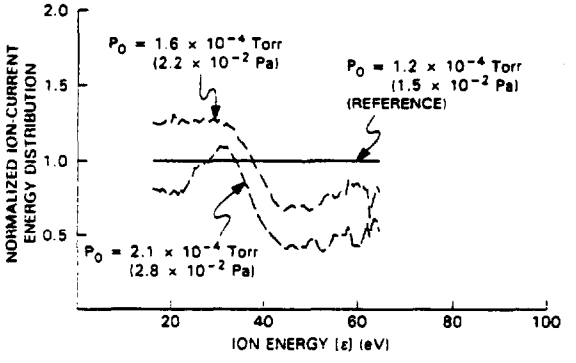

b. Normalized Ion-Current Energy Distributions

Fig. 5 Typical Ion-Current Energy Distribution Data

Uncertainty and accuracy considerations limit the energy range over which normalized data can be presented. On the low side the energy limit corresponds to anode potential (~16 V), which is considered to be close to ambient plasma potential. On the high side it is defined as the energy at which the measured reference ion current has dropped to 5% of its maximum value.

Ambient Pressure Effects

Figure 6a shows the measured effect of ambient pressure on the normalized ion-current energy distribution. The reference profile is the lowest pressure one. It should be noted that the normalized distributions shown in Fig. 6a are slightly different from the ones shown in Fig. 5b since the distributions shown in Fig. 6a are the mean profiles from several different tests (see Ref. 11) while Fig. 5b shows typical data obtained in a particular test series. Increasing the ambient pressure causes smaller ion currents to flow at energies greater than ~35 eV and greater ones at energies below this value. When the keeper was replaced by a starter electrode, similar results were obtained.

The corresponding effect of ambient pressure predicted using the scattering model (i.e. the right-hand side of Eq. (2) with z_1 = ~0 mm and z_2 = 180 mm, the distance between the cathode orifice and the ESA) are plotted in Fig. 6b. It should be noted that the predictions are dependent only on the difference in the neutral density profiles because only this difference appears in Eq. (2). The scattering model reflects only the effects of collisional losses on the ions and it includes no mechanism for ion production. The ion current distribution of Fig. 6b, therefore, shows a decrease over the entire energy range as neutral density is increased. Here, elastic collisions are represented by a hard-sphere model in which cross-sections are determined directly from the atomic radius of xenon and are independent of relative ion kinetic energy while the charge-exchange cross-section is only a weak function of this energy in this range.[12] The data in this figure, therefore, show a weak dependence on ion energy.

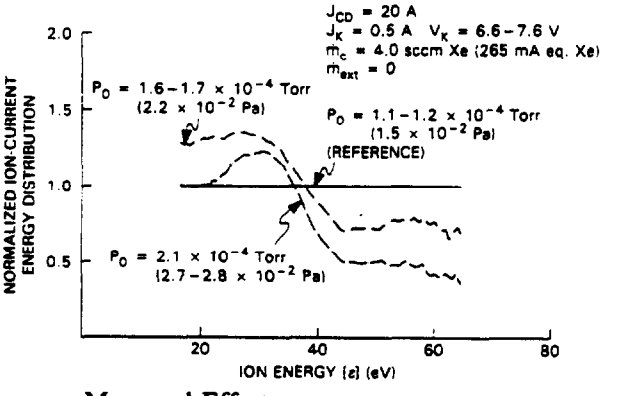

a. Measured Effects

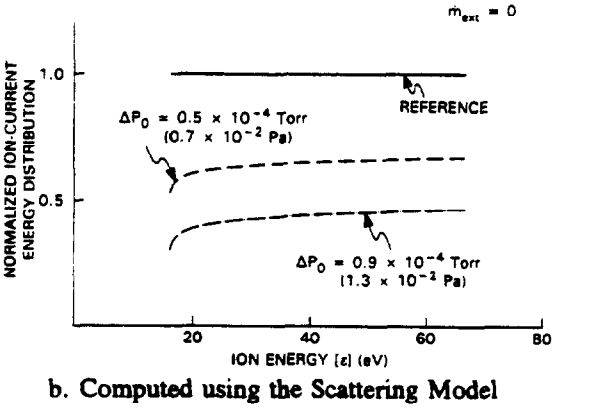

b. Computed using the Scattering Model

Fig. 6 Effect of Ambient Pressure on Ion-Current Energy Distributions

When the experimental results shown in Fig. 6a are compared with the predictions of Fig. 6b, one sees reasonable agreement for energies above ~45 eV while agreement is poor at energies below ~45 eV. There are, however, collisional mechanisms not reflected in the scattering model, which might explain this poor agreement at low energies. First, there could be collisions with neutrals which would cause ions to be scattered into the acceptance angle of the ESA or change their energy with almost no change in direction. Another mechanism, which could cause increases in ion currents at lower energies, would involve successive charge-exchange collisions with a small energy loss; the first occurring between high-energy ions and low-energy neutrals and the second between the resulting high-energy neutral and a low-energy, ambient-plasma ion. Overall, this would regenerate a high-energy ion. However, analysis shows these effects should be insignificant under the experimental conditions of Fig. 6. The first is small because the small ESA acceptance angle (8°)[10] should prevent most of the collection of lower-energy ions created via scattering. The second is small because the ion density is too low in the ambient plasma far from the cathode orifice to regenerate a significant high-energy ion current via charge-exchange collisions.

External Flow Rate Effects

The experimentally measured effects of external flow rate on normalized ion-current energy distributions are shown in Fig. 7a. Again these are mean curves and their precision is discussed in Ref. 11. These data are similar to those associated with ambient pressure changes in that the normalized distributions drop at the higher energies (> 30 to 35 eV) and increase at lower ones as the external flow rate and, hence, the neutral density is increased. However, the flow rate changes induce both more consistent trends and greater changes in the magnitudes of the normalized ion currents than the changes in ambient pressure.

Figure 7b shows the predicted effect of external flow obtained from the scattering model with z_1 = ~0 mm and z_2 = 180 mm. Again, ambient pressure is taken as arbitrary since only the difference in neutral density appears in the model. The plots of Fig. 7b show that scattering alone should cause the normalized energy distribution of ion currents to decrease over the entire range of energies and depend only slightly on the ion energy as the flow is increased. It should also be noted that the drops in the normalized distributions are smaller than those predicted for the changes introduced in

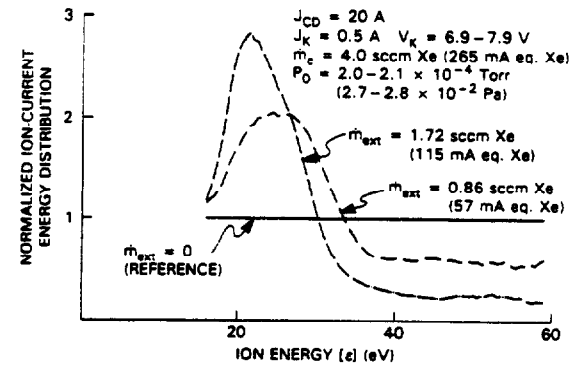

a. Measured Effects

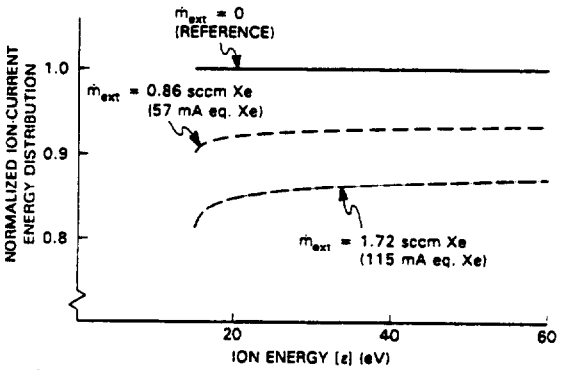

b. Computed using the Scattering Model

Fig. 7 Effect of External Flow Rate on Ion-Current Energy Distributions

ambient pressure because the changes in neutral density profiles introduced by the external flows were smaller.

Recall that increases in ambient pressure resulted in increases in neutral density globally that caused reductions in the normalized ion-current energy distribution at energies above ~45 eV, which were in fairly good agreement with the predictions of the scattering model. Comparison of the data of Figs. 6 and 7 shows, however, that increasing the neutral density near the cathode by increasing the external flow rate does not yield such good agreement between predicted and measured normalized ion-current energy distributions in this energy range. Since density changes induce only scattering losses in any MHD-like model, which involves energetic ion creation inside the cathode or orifice, a different model is required to explain the measured effects of density changes.

Neutral Density Effects in a Potential-Hill Model

The potential-hill model of energetic ion production was first postulated by Friedly and Wilbur.[3] When the electrons are extracted into a

region of high neutral density, a potential hill can develop as a consequence of extensive electron-impact ionization. As the process first starts and no significant net charge exists, electrons created inside the cathode are drawn out through the orifice and gain kinetic energies that are sufficient to ionize neutral atoms outside the cathode. After such ionization events, secondary electrons with low energies readily thermalize and escape this region because of their low mass. On the other hand, the more massive positive ions traveling at much lower speeds tend to accumulate thereby inducing electric fields and a potential hill like the one in Fig. 8. The potential-hill height continues to grow until the fields are sufficient to eject ions and/or trap the secondary electrons and a steady state is established. The ions created in this potential hill will gain kinetic energies as they fall through the electric fields that develop both upstream and downstream of the hill crest. It is postulated that the hill is located so close to the cathode orifice that it yields ions that appear to expand spherically from a point source. The existence of such hills has also been postulated in applications involving metal cathodes in vacuum arc[13] and hollow-cathode-based plasma contactors operating in the electron emission mode.[14] In this latter application, a hump in the potential profile was measured at low electron emission currents (a few amperes). For the potential-hill model, neutral atoms introduced downstream of the orifice can affect the flux of high-energy ions in competing ways; first, by scattering the ions thereby reducing the flux and second, by inducing increased ion production thereby increasing the flux.

A numerical model based on spherical 1-D geometry was developed to estimate the height of the potential hill. In the model, three groups of charged particles were considered: 1) mono-energetic, primary electrons ejected through the hollow cathode orifice and expanding into a downstream plasma, 2) ions created via ionization collisions between the primary electrons and neutral

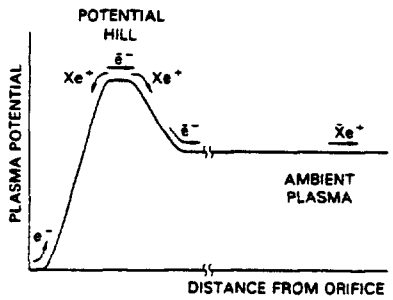

Fig. 8 Potential-Hill Model

atoms, and 3) low-energy electrons created via impact ionization and trapped in the hill region. The low-energy electrons are assumed to be characterized by a Maxwellian distribution. They can escape only when their partial pressure becomes sufficient to enable them to overcome electric field forces at the edges of the hill. Their density can be related to the ambient plasma density using the Boltzmann equation. In the model, it was also assumed that the potential in the hill region was uniform for simplicity. Details of the model development are described in Ref. 11.

When calculations were made, it was found that a potential hill height of ~30 V with respect to the cathode potential was required to neutralize the ion charge built up at the potential hill with low-energy, Maxwellian electrons trapped in the region. This height is consistent with the measured energies of the ions. However, changes in neutral density parameters had a negligible effect on peak potential. Also, it was argued that the model was deficient because it predicts ions are created only on the crest of the hill and will, therefore, all have the same energy (equal to the peak-to-cathode potential difference). These deficiencies can be addressed, however, by introducing the effect of charge-exchange collisions between the high-energy ions created on the hill and adjacent neutrals. The effects should be significant because charge-exchange mean free paths are expected to be in the order of millimeters near the orifice. These mean free paths are extremely small compared with 10-cm-order values in the ambient plasma.

The mechanisms involved can be understood by recognizing that ions created at the crest of potential hill undergo both acceleration and charge exchange as they fall through the potential gradient on the downstream side of the hill. The low-energy ions that result from this process gain kinetic energies only as they fall down the rest of the potential hill so they are detected with moderate energies. Increases in neutral density induce increases in charge-exchange rates and, therefore, in the currents of these lower-energy ions. It is noted that this effect will not be observed in any MHD-like model which does not involve the existence of a potential hill because all low-energy ions created by the charge-exchange collisions in the vicinity of orifice would be drawn upstream into the cathode by the adverse electric field.

When a model of this mechanism of moderate-energy ion production was used with measured density profiles, it showed that the effect of the scattering collisions that occur in the ambient plasma

dominate the charge-exchange effects that occur on the downstream of the potential hill. However, densities in the potential-hill region may be underestimated because they are extrapolated from downstream neutral-density measurements. In fact, the measured and computed results would be brought into agreement if greater neutral density changes near the cathode and lesser ones downstream of it were used in the numerical model.

Conclusions

Energy distributions of ion currents measured downstream of high-current hollow cathodes using an electrostatic energy analyzer reveal that either increasing the ambient pressure or adding external flow immediately downstream of a high-current hollow cathode induces an increase in the distribution of ion currents with moderate energies ($\varepsilon < -30$ to -35 eV) and a decrease in the distribution for high energies ($\varepsilon > -30$ to -35 eV). There is no mechanism by which the ion current at any energy can be increased significantly by increasing the downstream neutral density in the MHD model of energetic-ion production in high-current hollow cathodes. The potential-hill model of energetic-ion production does include a charge-exchange mechanism through which changes in neutral atom density could induce combined increases and decreases in moderate and high energy currents, respectively, through a charge-exchange mechanism.

Acknowledgment

This work was supported under Advanced Electric Propulsion Research Grant NAG3-1801 from the NASA Lewis Research Center.

References

1. Patterson, M.J., and Verhey, T.R., "5kW Xenon Ion Thruster Lifetest," AIAA Paper 90-2543, 21st International Electric Propulsion Conference, Orlando, FL, July 18–20, 1990
2. Brophy, J.R., and Garner, C.E., "A 5,000 Hour Xenon Hollow Cathode Life Test," AIAA Paper 91-2122, 27th Joint Propulsion Conference, Sacramento, CA, June 24–26, 1991
3. Friedly, V.J., and Wilbur, P.J., "High Current Hollow Cathode Phenomena," Journal of Propulsion and Power, Vol. 8, No. 3, May–June, 1992, pp. 635–643
4. Latham, P.M., Pearce, A.J., and Bond, R.A., "Erosion Processes in the UK-25 Ion Thruster," IEPC Paper 91-096, 22nd International Electric Propulsion Conference, Viareggio, Italy, October 14–17, 1991
5. Kameyama, I., and Wilbur, P.J., "Characteristics of Ions Emitted from High-Current Hollow Cathodes," IEPC Paper 93-023, 23rd International Electric Propulsion Conference, Seattle, WA, September 13–16, 1993
6. Kameyama, I., and Wilbur, P.J., "Zenith-Angle Distributions of Erosion Rates near High-Current Hollow Cathodes," AIAA Paper 96-3208, 32nd Joint Propulsion Conference and Exhibit, Lake Buena Vista, FL, July 1–3, 1996
7. Patterson, M.J., Rawlin, V.K., Sovey, J.S., Kussmaul, M.J., and Parkes, J., "2.3 kW Ion Thruster Wear Test," AIAA Paper 95-2516, 31st Joint Propulsion Conference and Exhibit, San Diego, CA, July 10–12, 1995
8. Polk, J.E., Patterson, M.J., Brophy, J.R., Rawlin, V.K., Sovey, J.S., Myers, R.M., Blandino, J.J., Goodfellow, K.D., and Garner, C.E., "A 1000 Hour Wear Test of the NASA NSTAR Ion Thruster," AIAA Paper 96-2784, 32nd, Joint Propulsion Conference and Exhibit, Lake Buena Vista, FL, July 1–3, 1996
9. Friedly, V.J., "Hollow Cathode Operation at High Discharge Currents," NASA CR-185238, April, 1990
10. Kameyama, I., and Wilbur, P.J., "Characteristics of Ions Emitted from High-Current Hollow Cathodes," NASA CR-195372, August, 1994
11. Kameyama, I., "Effects of Neutral Density on Energetic Ions Produced near High-Current Hollow Cathode," Ph.D. Dissertation, Colorado State University, Fall 1997
12. Rapp, D., and Francis, W.E., "Charge-Exchange between Gaseous Ions and Atoms," Journal of Chemical Physics, Vol. 37, No. 11, December 1962, pp. 2631–2645
13. Plyutto, A.A., Ryzhkov, V.N., and Kapin, A.T., "High Speed Plasma Beams in Vacuum Arcs," Journal of Experimental and Theoretical Physics (JETP), Vol. 20, pp. 328–337, 1965
14. Williams, J.D., and Wilbur, P.J., "An Experimental Investigation of Hollow Cathode-Based Plasma Contactors," NASA CR-187120, May 1991